

A Radio Census of Binary Supermassive Black Holes

S. Burke-Spolaor^{1,2*}

¹*Swinburne University of Technology Centre for Astrophysics and Supercomputing, Hawthorn VIC, Australia*

²*Australia Telescope National Facility, CSIRO, P.O. Box 76, Epping, NSW 1710, Australia*

ABSTRACT

Using archival VLBI data for 3114 radio-luminous active galactic nuclei, we searched for binary supermassive black holes using a radio spectral index mapping technique which targets spatially resolved, double radio-emitting nuclei. Only one source was detected as a double nucleus. This result is compared with a cosmological merger rate model and interpreted in terms of (1) implications for post-merger timescales for centralisation of the two black holes, (2) implications for the possibility of “stalled” systems, and (3) the relationship of radio activity in nuclei to mergers. Our analysis suggests that binary pair evolution of supermassive black holes (both of masses $\geq 10^8 M_\odot$) spends less than 500 Myr in progression from the merging of galactic stellar cores to within the purported stalling radius for supermassive black hole pairs. The data show no evidence for an excess of stalled binary systems at small separations. We see circumstantial evidence that the relative state of radio emission between paired supermassive black holes is correlated within orbital separations of 2.5 kpc.

Key words:

1 INTRODUCTION

Models of the Universe in which hierarchical merging dominates the growth of galaxies have strong predictions for the presence of binary supermassive black holes (SMBHs) at galaxy centres (e.g. Volonteri, Haardt, & Madau 2003). As galaxies containing such massive black holes collide, the central black holes are expected to inspiral and form a bound interacting system which will have a significant impact on the central galactic environment (Merritt 2006). In the time preceding their coalescence, these binary sources will be among the brightest of gravitational radiation sources detectable in the very low frequency (nHz to μ Hz) spectrum by pulsar timing experiments (e.g. Jenet et al. 2006). Such experiments are sensitive to both individual binary SMBHs with sub-parsec orbits and the stochastic gravitational wave background made up of the collective signal from binaries of mass $\sim 10^6 - 10^9 M_\odot$ (Detweiler 1979). In the mid-frequency spectrum (10^{-4} Hz to 0.1 Hz), the space-based Laser Interferometer Space Antenna (LISA)¹, is sensitive to gravitational waves from individual binary SMBH systems of mass $\lesssim 10^7 M_\odot$ in the later stages of their inspiral, coalescence, and post-coalescence ringdown. Predictions of the strength of this astrophysical gravitational wave background and the expected detection rates for LISA and pulsar timing of individual

black holes are based on parameterisations of merger rates and the SMBH population (Rajagopal & Romani 1995; Jaffe & Backer 2003; Wyithe & Loeb 2003; Enoki et al. 2004; Sesana, Vecchio, & Colacino 2008; Sesana, Vecchio, & Volonteri 2009), giving these gravitational wave detectors the potential to provide unique insights into the processes of galaxy formation.

In theoretical treatments, however, the evolution of post-merger central supermassive black holes still holds significant uncertainties. The steps in binary black hole formation and evolution were first laid out by Begelman et al. (1980). After a galaxy pair becomes virially bound, dynamical friction and violent relaxation drive the stellar cores containing the massive black holes (of masses m_1 and $m_2; m_1 > m_2$) to the centre of the merger remnant on roughly a dynamical friction time. When the cores have merged, the black holes independently experience dynamical friction against the merged core’s stellar environment. This further centralises each black hole, leading the system to become a bound pair at a separation where the enclosed stellar mass equals the total binary mass. If the stellar core is modelled as a single isothermal sphere with stellar density $\rho_*(r) = \sigma_v^2 / (2\pi Gr^2)$, this occurs when the black holes reach a orbital semi-major axis of

$$a_{\text{bin}} = \frac{3}{2} \frac{G(m_1 + m_2)}{\sigma_v^2}, \quad (1)$$

where σ_v is the velocity dispersion of the merger remnant. The length of time spent by black holes to reach this stage

* Email: sburke@astro.swin.edu.au

¹ See <http://lisa.nasa.gov>

follows the Chandrasekhar timescale for dynamical friction, and is limited by the inspiral timescale for the less massive black hole (cf. Lacey & Cole 1993):

$$t_{\text{df}} = 1.654 \frac{r^2 \sigma_v}{G m_2 \ln \Lambda}, \quad (2)$$

where we have assumed circular black hole orbits, and r is the orbital radius of the less massive black hole from the centre of the galactic potential. In such a system, we can assume a value for the Coulomb logarithm $\ln \Lambda \simeq 5$ (a non-circular orbit with ellipticity $\epsilon = 0.5$ will add a factor of roughly 0.5 to the timescale and the logarithm will be $2 \lesssim \ln \Lambda \lesssim 3$; e.g. Gualandris & Merritt 2008). The black holes will form a binary when $r = a_{\text{bin}}$.

The orbital evolution of the black holes proceeds further due to dynamical friction, however as the binary tightens and increases in velocity, dynamical friction becomes an ineffective means of energy transfer and the rate of inspiral slows. In this intermediate inspiral stage, there are significant uncertainties in both inspiral mechanism and timescale. Relaxing stars in radial orbits entering the “loss cone” of the massive binary (Frank & Rees 1976) will undergo 3-body interactions with the SMBH binary system and be ejected, carrying away angular momentum and further shrinking the binary orbit. However, without an additional mechanism for energy transfer or a means to efficiently refill the loss cone, the binary inspiral halts as the loss cone is emptied. Recognising the long timescale that loss cone re-population might take for binary systems, Begelman et al. (1980) suggest the possibility of gas ejection from the system or gas accretion onto the larger black hole, which will cause shrinkage in the binary orbit to conserve angular momentum (see also, e.g., Merritt & Milosavljevic 2005). If some intermediate process is able to sufficiently shrink the binary orbit, gravitational radiation will cause a binary with ellipticity $\epsilon = 0$ to coalesce in a timescale

$$t_g = \frac{5c^5}{256G^3} \frac{a^4}{m_1 m_2 (m_1 + m_2)}. \quad (3)$$

N-body simulations and semi-analytical models have manifested various intermediate inspiral processes (see, e.g., the extensive review of Colpi & Dotti 2009). The “last parsec problem” is the name given to the hurdle encountered by nearly all merger models in which the intermediate inspiral mechanisms have timescales sufficiently long that they are unable to bring the binary to a regime in which the emission of gravitational radiation can drive the black holes to coalescence in less than a Hubble time. If this is the case, there may be many instances of “stalled” binary objects which spend a large portion of their lifetimes with orbital radii within the range 0.01-10 pc (Yu 2002). A functional form for the stalling radius is estimated by Merritt (2006):

$$\frac{a_{\text{stall}}}{2 a_{\text{bin}}} = 0.2 \frac{m_1/m_2}{(1 + m_1/m_2)^2}. \quad (4)$$

If systems are unable to find the fuel to reach coalescence in less than the age of the Universe, then they may appear to stall indefinitely at orbits greater (thus GW frequencies lower, and amplitudes generally smaller) than those in the range detectable by either pulsar timing arrays or LISA. This would have dramatic consequences for GW detectors and for hierarchical formation models alike.

Since few small-orbit binary systems are known and electromagnetic tracers of post-merger galaxy cores are hard to identify, it has been difficult to study the post-merger dynamics of binary black hole systems. With only two confirmed sub-kpc double black holes serendipitously identified, (NGC 6240 at ~ 1 kpc, Komossa et al. 2003; 0402+379 at 7 pc, Rodriguez et al. 2006) there is little possibility to assess the physical mechanism responsible for driving binary systems into the phase when gravitational radiation dominates the binary inspiral. Observationally, there are several ways to identify galaxies with binary nuclei, which are reviewed briefly below (see also Komossa 2006 for a good overview).

Pairs of galaxies/quasars with small angular separations and similar redshifts, as well as galaxies which show disturbed structure and tidal tails in the optical and infrared, can indicate interaction between widely separated stellar cores containing SMBHs (e.g. Myers et al. 2008; De Propriis et al. 2007; Wen et al. 2008). Secondary signals that have been modelled as a consequence of a close or bound binary SMBH include quasi-periodic oscillations in flux density (OJ287, Valtonen et al. 1988), abnormal jet morphology such as helices or X-shaped radio jets (Saripalli et al. 2008; Lal et al. in press), spatial oscillations of an active galactic nucleus (3C66B, Sudou et al. 2003), and sources with double or offset broad/narrow line regions, implying active galactic nuclei (AGN) moving at high relative velocities to each other or to the host galaxy (e.g. Peterson et al. 1987; Comerford et al. 2008; Boroson & Lauer 2009; Decarli et al. 2010). In most of these cases, other explanations have better suited the observed characteristics of each source. However, spatially resolved systems such as 3C75, which shows two jet-emitting radio AGN cores, and NGC 6240 (Komossa et al. 2003) and other double X-ray emitting AGN (e.g. Wang & Gao 2010), are straightforward to identify and can provide a direct detection of a double SMBH system.

The core regions of radio-luminous AGN have been observed to show a distinct radio continuum spectrum which typically peaks at radio frequencies above ~ 1 GHz, giving core components a characteristically flat two-point spectral index ($\alpha > -0.5$, where radio flux $F_\nu \propto \nu^\alpha$) at GHz frequencies (e.g. Slee et al. 1994). This feature distinguishes the region most directly associated with the host black hole from the outer features such as larger scale jets or hotspots, which show power-law spectra generally at or steeper than $\alpha = -0.7$. Taking advantage of these unique spectral signatures of the core regions of radio-emitting AGN at high radio frequency (1 to 20 GHz) and the sub-milliarcsecond precision of observations using radio Very Long Baseline Interferometry (VLBI), it is possible to spatially resolve and identify AGN containing multiple cores using multifrequency gigahertz spectral imaging. This property has also been utilized to locate gravitationally lensed compact radio sources; if an AGN is lensed, it will also appear as a spatially resolved pair with equivalent radio continuum spectra (note that there is direct overlap in the target of such searches; because e.g. Wilkinson et al. 2001 found no lenses in 300 VLBI images, this implies no SMBH binaries were found, either).

In the case of a genuine physical pair, resolutions of 1 milliarcsecond are able to discern components with a projected spacing of above ~ 8.5 pc at *all* redshifts, and down to sub-pc resolutions for the nearest galaxies. This makes

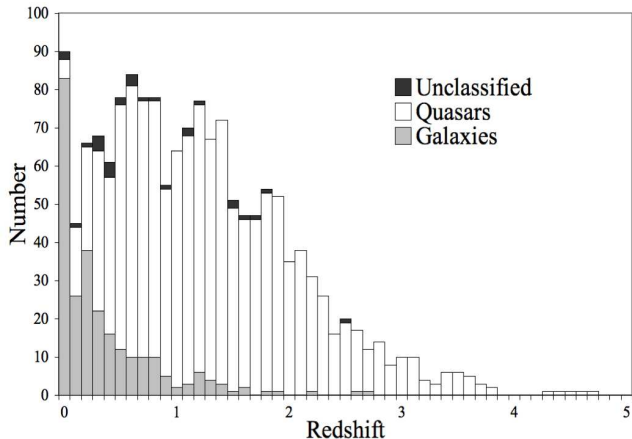


Figure 1. The redshift distribution of 1575 objects in our sample. The closest source is at $z = 0.000113$, while the highest redshift source is a quasar at $z = 4.715$.

VLBI observations well-suited to explore double supermassive black hole systems even at very small projected separations, and within post-merger galaxies that are otherwise unidentifiable as double or disturbed systems. Identification of double black holes in post-merger systems and binary black holes in the intermediate stage of inspiral will aid in showing evidence for stalling and may provide statistical estimates of the rate of SMBH inspiral at various phases.

This paper reports on the first systematic search of a large number of radio sources for spatially resolved binary radio AGN using archival VLBI data. We present a brief description of the archival data sample in §2, and summarise our search technique in §3. The candidates resulting from this search are assessed in §4. We outline an interpretive framework for making statistical estimates of inspiral timescales based on our detections in §5, and give the results of this analysis in §6. In §7 we discuss the analysis in terms of implications for black hole inspiral rates, stalling, radio core emission in the merging process, and implications for the pulsar-timing-detectable gravitational wave signal from SMBH binaries.

2 THE ARCHIVAL DATA SAMPLE

The data used in this search were extracted from the VLBI archives maintained online as the Goddard Space Flight Center astrometric and geodetic catalogues.² The catalogue version used was “VLBI global solution 2008a_astro,” which contains a large volume of calibrated VLBI data from 1980 to early 2008, including data from the VLBA calibrator surveys (Beasley et al. 2002; Fomalont et al. 2003; Petrov et al. 2005, 2006; Kovalev et al. 2007; Petrov et al. 2008). The catalogue contained observations unevenly sampled across 2.2 GHz to 43 GHz for 4169 radio sources. For our search technique, we are limited to sources observed at two or more frequencies, and to avoid potentially problematic intrinsic

² <http://lacerta.gsfc.nasa.gov/vlbi/solutions/> — Please see website and references therein for a complete description of original data sets

	2	5	8	15-24	43
5	96	—			
8	3101	94	—		
15-24	190	59	239	—	
43	34	0	37	132	—

Table 1. Frequency band pairs usable in our search; all frequencies are in units of gigahertz. The frequencies above refer to the rough observing band only. In total there were 3982 frequency pairs for 3114 sources.

source variability (see §3), we rejected frequency pairs which were observed at times separated by more than 35 days. Our sample was further culled because of software incompatibility for some data, and for the remaining dataset, observations were rejected if the images revealed data which contained no clear source above the noise. Three sources were removed because a literature searched revealed them to be Galactic HII regions or stars. In total, we were able to search data for 3114 sources.

Approximately half of the sources in our sample had redshift information available. The distribution for the 1575 sources of known redshift is shown in Fig. 1; the source types and redshifts were gathered from the NASA Extragalactic Database.³ The mean redshifts of our sample are $z_g = 0.402$, $z_q = 1.401$, and $z_{tot} = 1.226$ for galaxies, quasars, and all the sources with known redshift, respectively.

3 VLBI SEARCH FOR DOUBLE AGN

Our technique for identifying binary active galactic nuclei using VLBI is essentially a search for objects which show more than one flat-spectrum component. It requires morphological analysis and spectral index imaging across two or more frequencies to distinguish the nucleus of an object from its other components, such as complex extended structure or bright, unresolved hotspots along a jet. These other source components, as was previously noted, show systematically declining synchrotron spectra at $\alpha \lesssim -0.7$. The technique and the use of archival VLBI data require several precautions, primarily because both the accuracy of frequency-dependent flux density measurements and morphological fidelity of the radio image are important to this method.

We therefore take special precaution in considering AGN variability and coverage of the spatial-frequency ($u-v$) plane for the data sets. The variability exhibited by some radio AGN typically comes in two different flavours. Both particularly affect compact regions of emission with high brightness temperature, such as radio cores. The first is intra-day variability (IDV) due to propagation effects in the interstellar medium. This signal flickering can occur on sub-day timescales and exhibits a significant modulation index at frequencies below 5 GHz, causing fluctuations on average at the 1-10% level (e.g. Walker 1998; Lovell et al. 2008). Intrinsic variability in radio AGN cores is observed most significantly at frequencies above 5 GHz, and occurs on a wide range of timescales. Some radio AGN exhibit slow variations

³ NED, <http://nedwww.ipac.caltech.edu/>

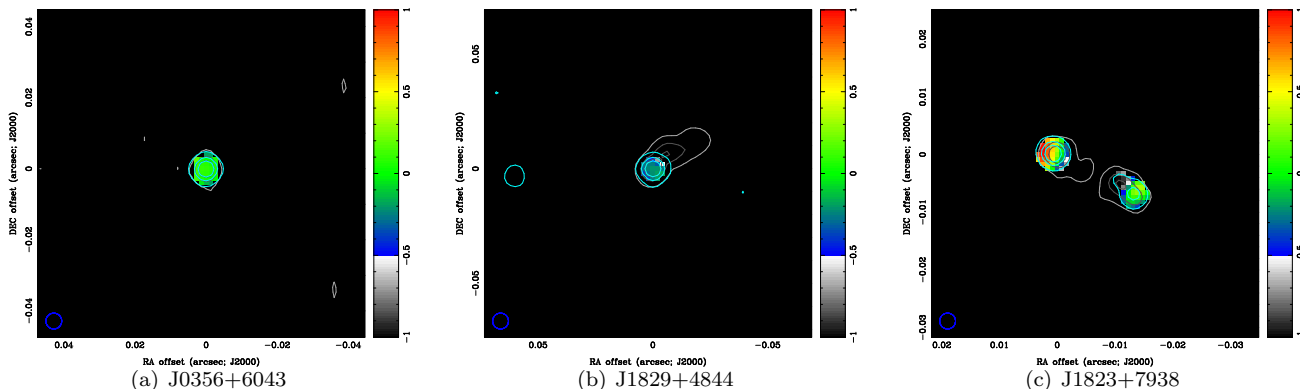


Figure 2. Two-frequency spectral index maps for sources tagged as (a) pointlike, (b) resolved, and (c) multiple flat-spectrum component sources. All maps show matched-resolution data. The color scale represents the spectral index calculated from two input maps of differing frequency. The color scale is linear in greyscale from $-1 < \alpha < -0.5$, and linear in color from $-0.5 < \alpha < 1$. The gray contours show the shape of the source at the lower frequency used to calculate the spectral index map, while blue contours trace the source morphology at the higher observing frequency used to calculate the spectral index map. These sources were randomly chosen from the source list for each category; all show matched-resolution data between 2.3 GHz (gray contours) and 8.4 GHz (blue contours). Contours in these plots are set at 2, 25, and 50 % of the peak flux at each frequency.

on timescales of years. The existence of such variations place limitations on the allowable temporal spacing between observations at different frequencies. Instantaneous multifrequency spectra will not be influenced by either effect, while observations spaced at less than the characteristic timescales of long-term AGN variability will allay the effects of a wandering high-frequency signal. For this reason we used only frequency pairs with a time separation of less than 35 days. Out of the 3982 usable frequency pairs in our data, 3447 were taken simultaneously, leaving 535 with an average difference in observation time of about 11 days.

All data processing was done using the MIRIAD software package (Sault, Teuben, & Wright 1993). For each frequency pair, we inverted the $u-v$ data, tapering the maxima of u and v to give a circular synthesised beam of the same size at the two frequencies. A manual inspection of $u-v$ coverage for the pairs ensured that the sources were sampled enough to provide an accurate representation of the source morphology at the tapered resolution. Images were cleaned, restored with the synthesised Gaussian beam of the tapered resolution to make images of 512x512 pixels, allowing a typical field of view 1.2 arcseconds to a side (though varying with the resolution of the observation). An estimate of the image noise level at each frequency was determined using an off-source region of each image. The number of frequency pairs we were able to use is detailed in Table 1.

The data were imaged in three ways for manual candidate searching. First, for each resolution-matched frequency pair, the full-field-of-view images at low and high frequency were plotted in greyscale with logarithmic contours beginning at three times the noise level of each image. Enhanced plots of the central image regions were made in a similar fashion, and a spectral index map of the inner regions was computed, calculating the spectral index pixel-by-pixel at any point in the image where the flux at both frequency bands was greater than three times the image noise. Spectral index images were superimposed with contours for each respective frequency, and the spectral index value was plotted as a colour image with a sharp desaturation break at

$\alpha = -0.5$ to enhance the appearance of flat-spectrum source components.

We then manually assessed each source, dividing sources into pointlike, resolved/extended, and multiple flat-spectrum component sources. Representative sources of each category are shown in Figure 2. Sources with multiple flat-spectrum components were considered preliminary candidates. In cases where the sources in multi-frequency images appeared displaced, a manual best-fit alignment was done and the source was reassessed. We considered a component to be “flat spectrum” if its two-point spectral index was $\alpha \gtrsim -0.6$ at any frequency pair, or if structure was visible at high frequency which was not detected at low frequency. As previously noted, sources which contained no detection above a 4σ noise level were removed from the sample.

The nature of preliminary candidates was then assessed by imaging all available observations of each candidate. Sources were then rejected from the candidate list if they satisfied any of the following:

- In the case of discrete compact flat spectrum components, if suspected components showed spectral steepening at later observation epochs (implying a false detection due to a young, evolving jet component).
- If an analysis of the time-dependent movement of suspected flat-spectrum source components revealed the component(s) as members of a steady outward (in some cases, superluminal) flow along a jet axis.
- If the full resolution image revealed beam sidelobes as the source of a spurious, flat-spectrum component.

Our search returned 12 candidates containing genuine multiple flat-spectrum components as discussed in more detail below.

4 CANDIDATES AND SEARCH RESULTS

Of the 3114 sources in our search, 68 percent were found to be pointlike at our frequency-matched resolution, while

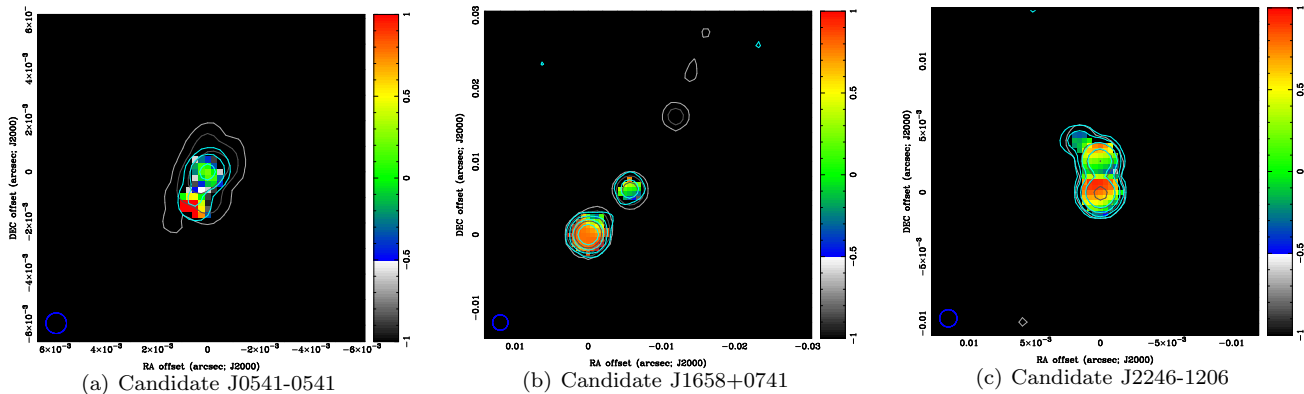


Figure 3. Example two-frequency spectral index and contour maps for three of the initial candidates described in §4.1. Coloring of the mapped data and contours are as in Fig. 2. Contours are set at 4, 16, 64, and 256 times the RMS image noise drawn from the respective frequency’s input image.

the remaining sources were identified as resolved or otherwise complex systems with only one flat spectrum component. The number of sources which exhibited multiple flat-spectrum components comprised less than 4 percent of the sample, and after the assessment of preliminary candidates, there remained only 12 candidate binary sources. As an example of our data quality for candidates, spectral and two-frequency contour images for three of the candidates below are shown in Figure 3. One candidate was the binary black hole candidate published by Rodriguez et al. (2006): 0402+379; an investigation of this source is available in their publication. We found that the remainder of our candidates appear to contain regions with active jet injection, which effectively gives rise to a population of contaminants for the radio spectral index mapping technique, in some cases requiring further data and analysis to distinguish such a source from a genuine binary black hole. Below we use our data and that available from the literature to further investigate each source and gather evidence for the presence of such processes, and not a binary black hole, in the sources.

Ultimately, we report the detection of no new binary systems. We have searched a sample of considerable size, finding only one spatially resolved binary black hole out of 3114 radio-bright AGN. Therefore, within the limitations of our search and data, we find 0.032% of sources in our sample in which a binary radio AGN was detected. The implications of this are discussed in later sections.

4.1 Candidates with active relativistic injection

Eleven of twelve candidates were rejected after the examination of all available data (in our data, the literature, or available online⁴) revealed that the multiple flat-spectrum components were part of a jet. These sources could be discriminated from a binary SMBH by proper (superluminal) motion, or by the resolving of the emission in higher resolution maps and alignment of the components with a more extensive outflow:

J0111+3906: The dynamical age of the source (370 yr, Owsianik, Conway, & Polatidis 1998, and the extendedness and alignment of the eastern component along the larger source structure indicate that it is a young jet.

J0541-0541: The southwestern flat spectrum component contains no compact emission at the high-resolution 8.4 GHz observation. This source is shown in Figure 3(a).

J0741+3112: The persistent total intensity and polarisation observations by Lister et al. (2009) clearly demonstrate that this source has a continuous outflow which is fuelling the flat spectrum hotspot apparent in our maps.

J1147+3501: Giovannini (1999) observe superluminal motion of the western flat-spectrum components.

J1223+8040: Pollack, Taylor, & Zavala (2003) indicate that there is a jet traversing our flat-spectrum components.

J1347+1217: The multiple flat-spectrum components are all members of an active superluminal outflow, as shown by the five year modelling of Lister et al. (2009).

J1459+7140: The southern component is fully resolved at our highest resolutions, and aligned with a small-scale jet emerging from the northern flat-spectrum component.

J1658+0741: The weaker flat-spectrum component of this source is resolved in our non-tapered images and is aligned with the northern jet, visible in Figure 3(b).

J1823+7938: The resolved structure of the easternmost component in our data and the proper motion analysis of Britzen et al. (2008) indicate that it is not a binary radio nucleus. This candidate is shown in Fig. 2(c).

J2246-1206: We conclude from the motion analysis of (Lister et al. 2009) that the northern component is a jet member. This candidate is displayed in Figure 3(c).

J2253+1608: Lister et al. (2009) show the western flat-spectrum component to be a jet member.

5 FRAMEWORK FOR INTERPRETATION

The use of radio data as a black hole indicator puts immediate constraints on both the physical properties and number of sources we will be sensitive to. We adopt the following expression for the number of sources expected to be found

⁴ We made use of the MOJAVE database at <http://www.physics.purdue.edu/MOJAVE>, which is maintained by the MOJAVE team Lister et al. (2009).

in our search:

$$N_{\text{exp}} = \sum_{i=0}^{N_s} f_{\text{bbh}}(z_i, m_{\text{lim}}) \cdot P_i \quad (5)$$

Here, N_s is the number of objects that have been searched. It is assumed that a target's redshift z is known (true for 1575 of our objects), and that it contains at least one detectable black hole of mass $M_{\bullet} > m_{\text{lim}}$.⁵ P represents the probability that we would detect a second black hole if the system is a binary, being the probability that the secondary black hole is both radio-emitting, and bright enough for a successful detection in our images. This term is explored in Sec. 5.1 below. The fraction of galaxies, f_{bbh} , containing a SMBH binary system at a redshift z' to which we are sensitive will be the cumulative number of galaxy mergers over the epoch at z' until the epoch at $z''[t_z - t_{\text{vis}}]$, where t_z is the age of the universe at redshift z' , and t_{vis} is the duration that a signature of a double black hole in the merging system is detectable in our search. Thus, if a binary stalls at a separation detectable by our technique (bounded by our observing resolution and the field of view of our images; see §5.3), galaxies that began to merge when the Universe was the age of z'' will still be occupied by a resolvable binary at z' . The occupation fraction for binaries at a resolvable separation is then given by:

$$f_{\text{bbh}}(z, m_{\text{lim}}) = \frac{\int_{z'}^{z''} N_{\text{mrg}}(z, m_{\text{lim}}) dz}{N_{\text{gal}}(z', m_{\text{lim}})}, \quad (6)$$

where N_{mrg} is the number of virialized galaxy pairs with SMBHs of masses above m_{lim} at the given redshift, while N_{gal} is the total number of galaxies at z' with SMBH masses greater than m_{lim} . The timescale of inspiral over the scales to which our data are sensitive (t_{vis}) can thus be estimated with a prediction or measurement of the redshift-dependent merger rate of galaxies containing supermassive black holes.

Whether we can identify a binary depends on factors explored in the sections below. The timescale over which we can resolve a binary is determined by our spatial sensitivity, the black hole masses and binary mass ratio; the relative time spent at various separations in a binary's inspiral depend on black hole mass. If the radio luminosity of the black holes somehow depends on the stage of the merger (for instance if the radio mechanism shuts down as the galaxies begin interacting, or ignites only after a binary coalescence), an additional factor needs to be considered in Eq. 5. However, because the evidence for a relationship between radio fuelling and merger events has until now been tenuous and estimates for an AGN timescale are so far inconclusive, we limit this uncertainty by employing two scenarios below that represent the most optimistic and the most pessimistic expectations for the state of radio luminosity in the two black holes.

⁵ Throughout our analysis we use a value $m_{\text{lim}} = 10^8 M_{\odot}$; here we make use of the observed property that radio-bright quasars have a distinct mass distribution: $\langle \log(M_{\bullet}/M_{\odot}) \rangle = 8.89 \pm 0.02$ with a lower cutoff around $10^8 M_{\odot}$ (e.g. McLure & Jarvis 2004). We probe only this most massive end of the black hole population, and for a double detection to be made, the second black hole must exceed a limiting mass $m_{\text{lim}} \geq 10^8 M_{\odot}$.

5.1 Supermassive Black Holes and Radio Emission

All our targets are radio sources detectable on parsec scales, and it follows that all contain at least one radio-emitting supermassive black hole. If a target is a binary system with a resolvable separation between the two black holes, due to our inspection techniques a second radio-emitting SMBH will have only been flagged as a candidate if its flux density exceeds four times the root-mean-squared noise (σ_{rms}) in its image. This $4\sigma_{\text{rms}}$ flux limit corresponds to a luminosity sensitivity limit of $L_{\text{lim}}(\sigma_{\text{rms}}, z)$. To predict the expected number of binary AGN to be found in our search and estimate a timescale for binary SMBH inspiral, we must first quantify the likelihood that the radio emission of a second black hole will exceed this luminosity limit.

The main unknown contributing to the discussion is how strongly the galactic and intergalactic environment relate to the production of radio AGN activity around the central black hole: that is, do the merger and mixing of gaseous, dusty, and stellar environments contribute strongly the production of radio activity? Below we assign two scenarios to bound assumptions at either end of extremes: 1) Pessimistic; the probability that a SMBH paired with a radio-emitting AGN is itself radio-emitting is no greater than the probability that a non-binary SMBH at the center of a massive galaxy would be radio-emitting, and 2) Optimistic; given a black hole that exists in a shared environment with a radio-emitting AGN, the probability of radio emission in the second black hole is unity.

Given that the black holes in the progenitors may not encounter significantly mixed environments until the binary has a relatively small separation, it is also possible that radio ignition is radially dependent. Regardless, we stress that for the third stage of inspiral in which theoretically the binary may stall, the stellar cores around the black holes have merged and the black holes will have shared many orbits within one another's sphere of influence and in a common environment.

5.1.1 Pessimistic scenario

We can make an estimate of the fewest number of binary sources we would expect to see by setting P equal to the integrated bivariate luminosity function of galaxies, $\psi(M, >L_{\text{lim}})$, where M represents the absolute optical/infrared magnitude of a galaxy. In this case we assume that mergers have no influence on the radio-active state of a black hole; that is, that the probability that the second black hole in a binary would have a detectable luminosity $L > L_{\text{lim}}$ is equivalent to the radio active fraction for non-merging galaxies selected from a random pool with $M_{\bullet} \geq m_{\text{lim}}$. We calculate P for each source using a log-linear interpolation of the integrated bivariate luminosity function of Mauch & Sadler (2007) for radio AGNs in galaxies with $-24 > M_K \geq -25$, taking such galaxies to be representative of our targets' host galaxies. As roughly 10% of the Mauch & Sadler (2007) sample have flat spectra (based on the measurements of Mason et al. (2009)), we expect that approximately 10% of their sources will be compact down to VLBI scales. To account for this we divide the space density given in their radio luminosity function by a factor of

10. For our 1575 sources with a known redshift, we find that in this scenario P has a mean and standard deviation of 0.4% and 1%, respectively.

5.1.2 Optimistic scenario

In the optimistic scenario, we consider that a SMBH in the presence of a radio AGN will itself be a radio-loud AGN. This scenario implies that when the two black holes share a common galactic environment, both black holes will be radio luminous if the conditions are fit for radio ignition; that is, both objects will be either radio-loud or not. We take as a given that one black hole is a detectable radio AGN in each of our images. To determine the detectability of a second SMBH in such a system (the probability that its observed luminosity is greater than L_{lim}), we would like to avoid the explicit use of e. g. relativistic beaming models, correlations between black hole mass and radio luminosity, and the levels of flux resolved by our baselines—the parameters of which are uncertain—by using an estimate derived from observations in which such effects are inherent.

We therefore take the secondary SMBHs in such systems to have a radio luminosity distribution equal to the luminosity distribution of solitary, flat-spectrum radio black holes, which will implicitly include beaming and mass-correlation effects. The use of the flat-spectrum population assumes that the emission observed in flat-spectrum radio sources is largely unresolved, and therefore scalable to the resolutions reached by our VLBI data. We adopt a probability density function for secondary black hole radio luminosities, $\rho(z, L) dL$, based on the redshift-dependent, flat-spectrum “pure luminosity evolution model” of Dunlop & Peacock (1990). We may then determine the probability that for a given object in the sample, a second black hole will have a luminosity above our detection threshold, L_{lim} . The probability that we would have detected the second black hole of a binary AGN is therefore:

$$P = \frac{1}{\rho_n} \int_{L_{\text{lim}}}^{\infty} \rho(z, L) dL. \quad (7)$$

The normalisation factor, $\rho_n = \int_{L_{\text{RL}}}^{\infty} \rho(z, L) dL$, sets the range of radio luminosities of radio-loud AGN. We set the lower luminosity bound of radio AGN at $L_{\text{RL}} = 10^{23} \text{ W Hz}^{-1} \text{ sr}^{-1}$, equal to that given by Padovani et al. (2009). Although the exact value of L_{RL} debatable, the average P value is not highly sensitive to the value of ρ_n if L_{RL} is decreased. For images in which the $L_{\text{lim}} < L_{\text{RL}}$, the probability of detection is set to one. For the 1575 known-redshift sources in this scenario, P has a mean and standard deviation of 57.9% and 23.7%, respectively.

5.2 Host Properties and Limiting Radii

The predicted binary formation radii and stalling radii mark key points in possible inspiral rate changes for a post-merger system. In order to determine what stage of inspiral we have probed with our spatial sensitivity limits, we require an estimate of the predicted typical a_{bin} and a_{stall} for our sample. As mergers between less massive galaxies are expected to be more common than high mass mergers, for this study we expect the least massive (and most common) merger probed

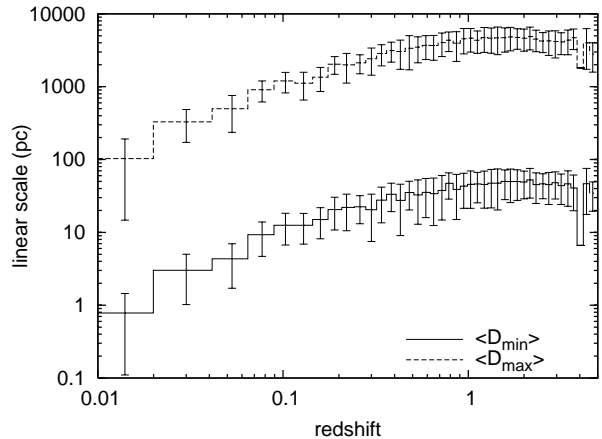


Figure 4. The upper and lower bounds of the average linear scales searched as a function of redshift. The error bars represent the standard deviation of $\langle D_{\text{min}} \rangle$ and $\langle D_{\text{max}} \rangle$.

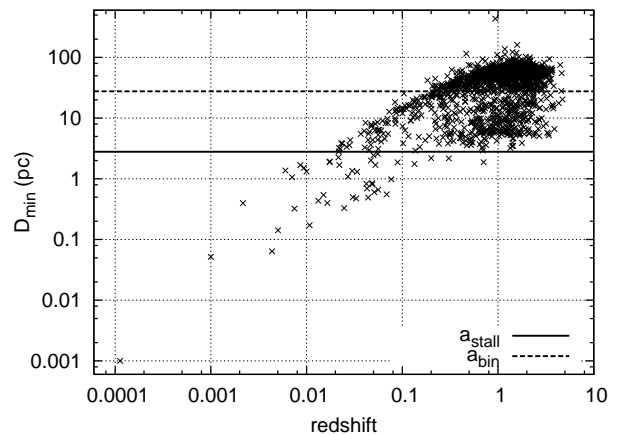


Figure 5. The minimum resolvable linear scale for each of the sources of known redshift in our sample. Overplotted are the predicted black hole binary formation radius and stalling radius for two $10^8 M_{\odot}$ black holes. Note that for a binary in a circular orbit, these radii correspond to a maximum projected separation of twice each value.

in our sample to involve two black holes of $10^8 M_{\odot}$. Relevant progenitor galaxy properties can be calculated to estimate the characteristic scales (e.g. stalling radius, binary formation radius) that our study probes. Using two black holes of mass $10^8 M_{\odot}$, each progenitor’s velocity dispersion, $\sigma_v \sim 187 \text{ km s}^{-1}$, and bulge mass, $M_{\text{host}} \sim 6.63 \times 10^{10} M_{\odot}$, can be estimated by the $M_{\bullet} - \sigma_v$ relation of Ferrarese & Merritt (2000) and the $M_{\bullet} - M_{\text{bulge}}$ relation of Haring & Rix (2004), respectively. If the black holes do not accrete a significant fraction of their mass during inspiral, the post-merger galaxy will contain a black hole of $2 \times 10^8 M_{\odot}$ and an implied velocity dispersion of $\sigma_v \sim 216 \text{ km s}^{-1}$. The binary formation radius for our typical system is thus $a_{\text{bin}} = 27.7 \text{ pc}$, while the stalling radius is $a_{\text{stall}} = 2.8 \text{ pc}$ (equations 1, 4). In the earliest stage of merger, the virially bound galaxy pair will have a projected separation $\lesssim 7 \text{ kpc}$. We note that while these radii are the characteristic values for the sources in the sample, more massive (and less common) mergers be-

tween $10^9 M_\odot$ black holes will have larger radii by a factor of ~ 10 .

5.3 Spatial Limits of the Search

Our technique resolves a large range of spatial scales, over which an inspiral rate will undergo several changes. To estimate post-merger black hole evolutionary timescales we must determine the projected spatial separation range that our data set is sensitive to. For the 1575 sources of known redshift, the average maximum and minimum projected linear spatial sensitivities ($\langle D_{\max} \rangle$, $\langle D_{\min} \rangle$, both in units of parsec) as a function of redshift are plotted in Figure 4. The sources are binned in increments matching the redshift steps of the Millennium Simulation snapshots (see §5.4; each step spans an average of 300 Myr).

The observed scales are derived as follows: the minimum and maximum linear projected separation between two objects that we are sensitive to are set by our angular resolution, θ_r , and half the field of view of our search maps, given that one AGN will lie at the pointing centre of the observation. Using the redshift of each source and a flat-universe cosmology with $H_0 = 72 \text{ km s}^{-1} \text{ Mpc}^{-1}$, $\Omega_m = 0.27$, and $\Omega_\Lambda = 0.73$, we calculate d_z/θ_z , the distance (in pc) per milliarcsecond at that redshift on the plane of the sky. Our smallest resolved size for that source is then $D_{\min} = d_z \theta_r / \theta_z$ parsecs (D_{\min} for individual sources are plotted in Figure 5). Because we searched images of 512 pixels to a side and the synthesised restoring beam is 3 pixels in breadth, the maximum linear scale we are sensitive to is:

$$D_{\max} = \frac{512 \theta_r}{6} \cdot \frac{d_z}{\theta_z} \text{ parsecs.} \quad (8)$$

This value represents the largest scale size to which the search of each source is complete. For sources with known redshift, the sample averages were $\langle \theta_r \rangle = 6.5 \text{ mas}$, $\langle D_{\min} \rangle = 40 \pm 25 \text{ pc}$ and $\langle D_{\max} \rangle = 3415 \pm 2133 \text{ pc}$.

The limited spatial separation window over which we have searched each source for a double AGN and the potential for drastic changes in inspiral rate at various stages of the binary evolution compel us to divide our measurement of inspiral rates into three stages. We do so by segregating the sources by their spatial resolution into groups which represent sensitivity to three stages of merger evolution: the stage at which the stellar cores have not yet merged (merger stage 1), the stage leading to binary formation in which the cores merge and the binary forms (stage 2), and the final stage to which we can probe spatially, in which the black holes are a binary and evolve to the predicted stalling radius (stage 3). In each of these groups, we consider that a linear resolution of $D_{\min} = a_{lo}$ will allow the detection of sources with an orbital semi-major axis of a_{lo} roughly 80% of the time, assuming systems with a random distribution of inclination angles. By setting the constraint on a group that $D_{\min} < a_{lo}$, we ensure that the searched nuclei in that group will be sensitive to binaries with axis $a \geq a_{lo}$ for $> 80\%$ of the pair's orbit. Each group is statistically sensitive in this way to pairs with an orbital axis of up to $\langle D_{\max} \rangle$ of the group.

The three groups are divided at (1) $27.7 < D_{\min} < 120$ parsecs, (2) $2.8 < D_{\min} < 27.7$ parsecs

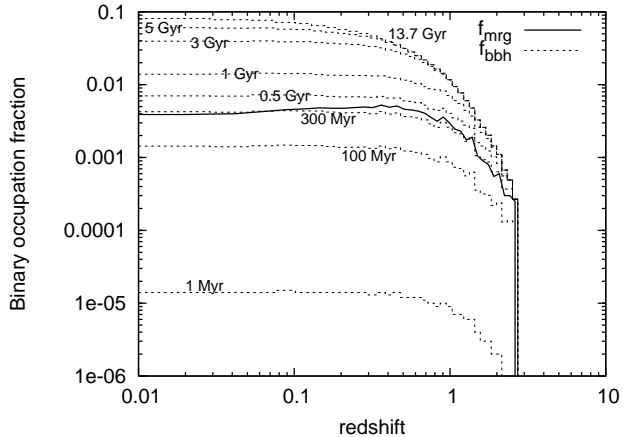


Figure 6. The redshift-dependent fraction of galaxies containing binary or double SMBH black hole systems for various inspiral times, based on the merger rate predictions of De Lucia & Blaizot (2007) for mergers with black holes of masses $m_1, m_2 \geq 10^8 M_\odot$.

(sensitivity down to our limiting a_{bin}), and (3) $D_{\min} < 2.8$ parsecs (giving sensitivity down to the minimum a_{stall}). Because sources with very high resolution observations will not have a large value of D_{\max} and thus not probe large separations, the source group (3) is not included in (2), and in turn these two groups are not included in (1). The divisions give a sensitivity to binaries at separations over three ranges of scales:

- (1) $120 < a < 4757$ parsecs
- (2) $27.7 < a < 2519$ parsecs
- (3) $2.8 < a < 450$ parsecs

There were 1035, 497, and 43 sources in groups one, two, and three, respectively.

5.4 Galaxy Merger Rates

The merger rate of galaxies containing SMBHs given a Λ CDM universe in which merging is the primary mechanism for galaxy growth can be predicted using results from the Millennium Simulation (Springel et al. 2005). The Millennium simulation is a large-scale N-body simulation which tracked the evolution of dark matter halos in a co-moving cubic volume $500 \text{ Mpc } h^{-1}$ to a side ($h = H_0/100 \text{ km s}^{-1} \text{ Mpc}^{-1}$). De Lucia & Blaizot (2007) applied a semi-analytical prescription to the Millennium simulation to track the evolution and merger histories of individual galaxies within the Millennium volume. Their catalogue can be queried through an online interface.⁶

Using the Millennium catalogue, we constructed the redshift-dependent distribution of galaxies and mergers in which each galaxy contains a supermassive black hole of $M_\bullet > 10^8 M_\odot$. For comparison with the black hole binary occupation fraction, we show these values as a pair fraction, where $f_{\text{mrg}} = N_{\text{mrg}}/N_{\text{gal}}$; here, N_{mrg} and N_{gal} are the number of mergers and the total number of galaxies, respectively, with $M_\bullet > 10^8 M_\odot$ at the given simulation snapshot.

⁶ See <http://www.g-vo.org/Millennium>

A “merged” pair in the Millennium Simulation and the De Lucia & Blaizot framework is a pair which has become gravitationally bound in the ~ 300 Myr between two adjacent snapshots.

Figure 6 shows the redshift-dependent pair fraction for $m_{\text{lim}} > 10^8 M_{\odot}$ and the corresponding black hole binary occupation fraction (computed from eq. 6) for a range of inspiral times. The merger distribution peaks at a redshift of about $z = 0.7$.

6 LIMITS ON INSPIRAL TIMESCALES

Following Eq. 5, for the merger stage groups with no SMBH binary detections, we place an upper limit on t_{vis} at $N_{\text{exp}} = 0.5$. The one source in which a binary black hole was detected is part of the second merger stage group; for this group/region only are we able to make a measurement of (rather than put a limit on) t_{vis} , with errors bounding where t_{vis} gives a value of $0.5 < N_{\text{exp}} < 1.5$.

The timescale measurements for the optimistic scenario are summarised in Figure 7, which illustrates the number of black holes expected to be found in each group as a function of t_{vis} , and Table 2, which gives the numerical values of our limits. Under the pessimistic set of assumptions, we would not expect to see any sources, given that even with $t_{\text{vis}} = 1/H_0$, we find $N_{\text{exp}} = 0.025, 0.20$, and 0.16 for groups 1, 2, and 3, respectively. The implications of this will be discussed in the next section.

In Table 2 we report the timescales measured from both our 1575 sources of known redshift, and from the full sample with an assumed redshift distribution. While we do not use the less reliable “full sample” timescale values in the analysis below, we stress the limiting power of the sample if we were to have a full sample with measured redshifts, by assuming the remaining sources have a redshift distribution equivalent to the other 1575. This has the effect of roughly doubling N_{exp} for each group, and as such works only to lay more stringent limits on t_{vis} .

Finally, although the number of sources in group one was the largest, these sources also had a tendency to be of higher redshift, with a net effect of fewer expected detectable binary black holes due to the lower merging fraction of SMBH hosts at redshifts $z \gtrsim 1$. For stalling studies, the observation of low-redshift sources is therefore doubly beneficial: not only does it allow smaller scales to be resolved in the sources due to their proximity, but it affords a higher predicted success rate due to the increased merger rate of SMBH-hosting galaxies at low redshift.

7 DISCUSSION

The question we aim to answer with this search is whether there is observational evidence for stalled supermassive binary black hole systems: that is, what is the evolution timescale down to the stalling radius for a post-merger supermassive black hole pair? For our methods, this question is intertwined with how closely correlated the radio emission is between two black holes in a pair. Our sample allows us to address this correlation and inspiral timescales over three stages of post-merger SMBH pair evolution. This

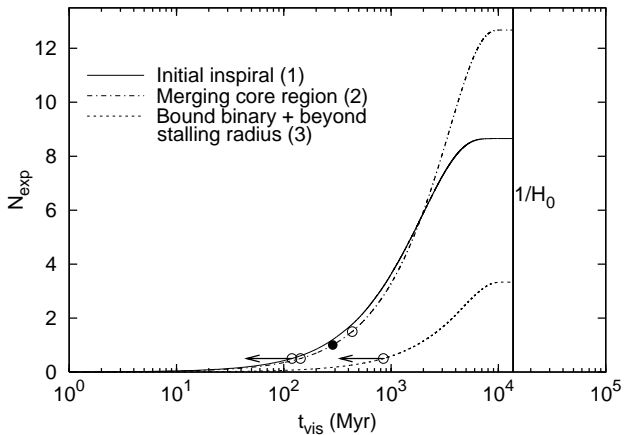


Figure 7. The cumulative expected number of sources and limits on the inspiral timescale for each spatial-sensitivity limited group using the optimistic scenario (§5.1.2) in which given one radio-active black hole in a binary, the second will also be radio-emitting. For groups 1 and 2, the upper limit set on t_{vis} is marked with an arrow, while for group two the measured value of t_{vis} is marked by a filled circle, with open circles indicating the error range.

	Known redshift	Full sample
Group 1	<0.119	<0.060
Group 2	0.286^{+148}_{-143}	0.143
Group 3	<0.846	<0.416
Net	<1.25 Gyr	<619 Myr

Table 2. A summary of the t_{vis} measurements (in Gyr) placed by our known redshift sources (1575) and the full sample with an assumed redshift distribution (3114 total). The values given are for the set of optimistic radio luminosity assumptions (§5.1). Groups 1–3 are as detailed in §5.3. Although the groups overlap in their linear separation sensitivities, we quote a “Net” timescale that gives a limit on the total timescale of inspiral from galaxy virialization to SMBH separations beyond the stalling radius.

is discussed below, followed by a brief consideration of the consequences of our results for the detection of gravitational waves from SMBH binary systems by pulsar timing arrays.

7.1 Post-merger efficiency, radio ignition, and SMBH binary stalling

The timescales measured for our three merger stages represent the time a pair’s orbital separation takes to evolve through the spatial sensitivity window of each stage. For our merger stage groups one and two (\sim virialisation down to SMBH binary formation), it is expected that purely dynamical friction will act on the black holes. Formally, the dynamical friction timescale in equation 2 over the range probed by our first and second merger stage groups is ~ 3.7 Gyr and 900 Myr, respectively, for an object of mass $10^8 M_{\odot}$.

For merger stage group one, the optimistic scenario timescale limit is smaller than the dynamical friction timescale by a factor of ~ 30 . From this disagreement, it follows that one of the following must be true: 1) the relative radio state of two SMBHs in merging galaxies is

not strongly correlated before the hosts’ stellar cores have merged, and/or 2) The centralisation of supermassive objects in a post-merger system is highly efficient (in excess of dynamical friction).

Considering merger stage group two, in which we have detected one binary SMBH, the timescale under the optimistic set of assumptions gives a value more consistent (a factor of ~ 2 within the error bounds) with dynamical friction. Because in the pessimistic limit we would not expect to see any sources, it is implicit that the pessimistic assumptions are not strictly valid for this stage of merger. This is furthermore indicative of some radial dependence of the relative radio state of two SMBHs in a post-merger environment, such that the SMBHs have a correlated radio active state at later stages of SMBH inspiral, after the pair has shared a common galactic environment for many orbits.

We have set the cutoff for the third merger stage group to be sensitive to the theoretical stalling radius of Merritt (2006). While the limits that we can place on this stage of merger are the least stringent due to the small source count in the limiting group, they represent the first observational exploration of stalling. If the evidence exhibited by merger stage group 2 holds—that the relative radio state between two black holes is more strongly correlated at late stages of binary evolution—our results are in agreement with a progression through the stalling radius in much less than a Hubble time; that is, we find no evidence for systematic stalling of supermassive binary black hole systems. These results, however, exist with the significant caveat: if the most pessimistic assumptions are true, we would not expect to see any paired SMBHs regardless of the length of post-merger inspiral.

As previously noted and reflected in table 2, we have only used the information from roughly half of our sources to acquire timescale measurements. The lack of detections in the additional 1539 sources suggests that the measured limits will only be more stringent, however would be highly dependent on the redshift distribution of the remaining sources.

7.2 Consequences: gravitational wave background and pulsar timing arrays

The measured inspiral timescales and lack of evidence for stalled supermassive systems are pertinent results for pulsar timing arrays, which are sensitive to the most massive of binary mergers such as those explored by this study. While we have primarily accentuated the brevity of timescale to pass through the stalling stage, we note also that the timescales measured for merger group two (in concert with time spent at other separations) are sufficiently large that they may have non-negligible effects on predictions of the gravitational wave background signature in the local Universe from SMBH binaries. Typically, estimates of expected binary black hole contributions assume efficient or instantaneous inspiral into the gravitational wave regime (e.g. Sesana, Vecchio, & Colacino 2008), using merger rates as binary coalescence rates. The inspiral times measured here may cause the galaxies merging at a redshift of 0.7, at which the merger distribution peaks, to emit gravitational radiation at a much later epoch, causing a larger expected amplitude for the astrophysical gravitational wave

background than previously estimated. In addition, it is likely that this effect would cause an increase in the predicted number of supermassive binary sources whose gravitational radiation is strong enough to be resolved from the gravitational wave background by pulsar timing arrays (Sesana, Vecchio, & Volonteri 2009).

8 SUMMARY

We have performed a search of 3114 active galactic nuclei for the presence of double SMBH systems using a multi-frequency radio imaging technique. Of the sources searched, only 0402+379 was apparent with our method as a binary AGN. While this source has already been put forward as a binary black hole in Rodriguez et al. (2006), this search represents a significant enough statistical sample with which to interpret the existence of this source in the broader cosmological context of binary supermassive black holes.

This search has probed estimates of the inspiral timescale for binary black holes of $m_1, m_2 \geq 10^8 M_\odot$. For the 1575 sources that had redshift information with which to discern the linear scales probed in the host galaxy, we obtained timescale estimates for the inspiral of binary systems in three ranges of binary separation. We have demonstrated observational evidence against stalled binary black hole systems by demonstrating that: 1) at late stages of SMBH pair inspiral, the two black holes are more likely to be in a similarly radio-active state, and 2) SMBH binaries proceed from separations of $a \simeq 500$ parsecs to within the stalling radius estimates of Merritt (2006) in less than ~ 0.5 Gyr. The implications of this are that supermassive binary systems do not stall indefinitely at such radii, suggesting there is a yet undetermined mechanism by which the black holes are able to dispense energy to the surrounding environment and proceed to coalescence.

The results of this study come with the caveat that they stem on very small-number statistics; that is, we detected only one binary AGN in the analysis, and due to unmeasured redshifts, we were unable to use roughly half of the sources searched in the statistical analysis. Definitive studies of this type for large numbers of AGN will become possible with the large collecting area, dense instantaneous $u-v$ coverage, and long baselines of the planned Square Kilometer Array.

9 ACKNOWLEDGEMENTS

This publication is part of the doctoral thesis of SBS. The author would like to acknowledge the support of her supervisors M. Bailes, and particularly R. N. Manchester for their assistance in revising and preparing this manuscript. The author thanks M. Spolaor for his continued support, and Prof. I. Browne for his insightful feedback on this manuscript. SBS acknowledges the Astronomical Society of Australia for financial travel assistance that contributed to the completion of this paper.

REFERENCES

- Beasley A. J., Gordon D., Peck A. B., Petrov L., MacMillan D. S., Fomalont E. B., Ma C., 2002, *AJ Supp.*, 141, 13

- Begelman M. C., Blandford R. D., Rees M. J., 1980, *Nature*, 287, 307
- Borson T. A., Lauer T. R., 2009, *Nature*, 458, 53
- Britzen S., et al., 2008, *A and A*, 484, 119
- Colpi M., Dotti M., to appear in *Advanced Science Letters* (arXiv:0906:4339)
- Comerford J. M. et al., 2008, astro-ph arXiv:0810.3235, *submitted to ApJ*
- De Lucia G., Blaizot J., 2007, *MNRAS*, 375, 2
- De Propriis R., Conselice C. J., Liske J., Driver S. P., Patton D. R., Graham A. W., Allen P. D., 2007, *ApJ*, 666, 212
- Decarli R., Dotti M., Montuori C., Liimets T., Ederoclite A., 2010, *ApJ Letters*, 720, 93
- Detweiler S., 1979, *ApJ*, 234, 1100
- Dunlop J. S., Peacock J. A., 1990, *MNRAS*, 247, 19
- Enoki M., Inoue K. T., Nagashima M., Sugiyama N., 2004, *ApJ*, 615, 19
- Ferrarese L., Merritt D., 2000, *ApJ Letters*, 539, L9
- E. Fomalont, L. Petrov, D. S. McMillan, D. Gordon, C. Ma, *AJ*, 126, 2562
- Frank J., Rees M. J., 1976, *MNRAS*, 176, 633
- Giovannini G., Taylor G. B., Arbizzani E., Bondi M., Cotton W. D., Feretti L., Lara L., Venturi T., 1999, *AJ*, 522, 101
- Gualandris A., Merritt D., 2008, *ApJ*, 678, 780
- Haring N., Rix H., 2004, *ApJ Letters*, 604, L89
- Jaffe A. H., Backer D. C., 2003, *ApJ*, 583, 616
- Jenet F. A., and 9 co-authors, 2006, *ApJ*, 653, 1571
- Komossa S., Burwitz V., Hasinger G., Predehl P., Kaastra J. S., Ikebe Y., *ApJ*, 582, L15
- Komossa S., 2006, *Memorie della Societa Astronomica Italiana*, 77, 733
- Y. Kovalev, L. Petrov, E. Fomalont, D. Gordon, 2007, *AJ*, 133, 1236
- Lacey C., Cole S., 1993, *MNRAS*, 262, 627
- Lal D. V., and 7 co-authors, in press, arXiv:0904.2725
- Lister M. L., et al., 2009, *AJ*, in press, astro-ph arXiv:0812.3947
- Lovell J. E. J. et al., astro-ph arXiv:0808.1140v1
- Mason B. S., Weintraub L., Sievers J., Bond J. R., Myers S. T., Pearson T. J., Readhead A. C. S., Shepherd M. C., 2009, *ApJ*, 704, 1433
- Mauch T. & Sadler E. M., 2007, *MNRAS*, 375, 931
- McLure R. J., Jarvis M. J., 2004, *MNRAS*, 353, L45
- Merritt D., 2006, *ApJ*, 648, 976
- Merritt D., Milosavljevic M., 2005, *Living Rev. Relativity*, 8, 8
- Myers A. D., and 7 co-authors, 2008, *ApJ*, 678, 635
- Owsianik I., Conway J. E., Polatidis A. G., 1998, *A and A Letters*, 336, L37
- Padovani P., Mainieri V., Tozzi P., Kellermann K. I., Fomalont E. B., Miller N., Rosati P., Shaver P., 2009, *ApJ*, 694, 235
- Peterson B. M., Korista K. T., Cota S. A., 1987, *ApJ Letters*, 312, 1
- L. Petrov, Y. Kovalev, E. Fomalont, D. Gordon, 2005, *AJ*, 129, 1163
- L. Petrov, Y. Kovalev, E. Fomalont, D. Gordon, 2006, *AJ*, 131, 1872
- L. Petrov, Y. Kovalev, E. Fomalont, D. Gordon, 2008, *AJ*, in press
- Pollack L. K., Taylor G. B., Zavala R. T., 2003, *ApJ*, 589, 733
- Rajagopal M., Romani R. W., 1995, *ApJ*, 446, 543
- Rodriguez C., Taylor G. B., Zavala R. T., Peck A. B., Pollack L. K., Romani R. W., 2006, *ApJ*, 646, 49
- Saripalli L., Subrahmanyam R., Laskar T., Koekemoer A., 2008, *accepted to From Planets to Dark Energy: The Modern Radio Universe*, PoS(MRU)130
- Sault R. J., Teuben P. J., and Wright M. H. C., 1995, *ASPC*, 77, 433
- Sesana A., Vecchio A., Colacino C. N., 2008, *MNRAS*, 390, 192
- Sesana A., Vecchio A., Volonteri M., 2009, *MNRAS*, 394, 2255
- Slee O. B., Sadler E. M., Reynolds J. E., Ekers R. D., 1994, *MNRAS*, 269, 928
- Springel V. et al., 2005, *Nature*, 435, 629
- Sudou H., Iguchi S., Murata Y., Taniguchi Y., 2003, *Science*, 300, 1263
- Valtonen M., and 8 co-authors, 1988, *LNP*, 307, 68
- Volonteri M., Haardt F., Madau P., 2003, *ApJ*, 582, 559
- Walker M. A., 1998, *MNRAS*, 294, 307
- Wang J., Gao Y., 2010, *Res. in Astronomy and Astrophysics*, 10, 309
- Wen Z. L., Liu F. S., Han J. L., 2008, *accepted to ApJ*, arXiv:0810.5200
- Wilkinson P. N., Henstock D. R., Browne I. W., Polatidis A. G., Augusto P., Readhead A. C., Pearson T. J., Xu W., Taylor G. B., Vermuelen R. C., 2001, *Physical Review Letters*, 85, 584
- Wyithe J. S. B., Loeb A., 2003, *ApJ*, 590, 691
- Yu Q., 2002, *MNRAS*, 331, 935